



# Synthesis of silicon carbide (SiC) micro-particles from PCB waste through dry milling as a candidate for microfluidic particles in quenching media

Rifqi Aditya Rehanda<sup>1,\*</sup>, Myrna Ariati Mochtar<sup>1</sup>, Wahyuaji Narottama Putra<sup>1</sup>

<sup>1</sup> Department of Metallurgical and Materials Engineering, Faculty of Engineering, Univeritas Indonesia, Depok, West Java, 16424, Indonesia.

\* Correspondence: rifqi.aditya01@ui.ac.id

Received Date: January 11, 2025

Revised Date: February 28, 2025

Accepted Date: February 28, 2025

## ABSTRACT

**Background:** The increasing demand for electronic devices due to technological advancements has led to a rise in electronic waste, particularly printed circuit boards (PCBs). This study aims to utilize PCB waste, which contains non-metal particles such as silicon (Si) and silicon carbide (SiC), to enhance the thermal conductivity of cooling media. **Methods:** The research process began with the crushing of PCBs, followed by leaching with 1M HCl for 24 hours. Subsequently, pyrolysis was conducted using argon at 500°C for 30 minutes. The resulting PCB particles were then subjected to dry milling in a planetary ball mill with varying ball-to-powder ratios of 1:10, 1:30, and 1:50 for durations of 10 and 20 hours, using steel balls. The milled particles were characterized using X-ray fluorescence (XRF), X-ray diffraction (XRD), and particle size analysis (PSA). **Findings:** XRF analysis revealed that SiO<sub>2</sub> was the predominant compound. XRD results indicated significant SiC phase growth in the 1:50 parameter with a 20-hour milling time. PSA results showed the smallest particle size of 627.6 d.nm with a polydispersity index of 0.047 in the 1:10 variable with a 20-hour milling time. **Conclusion:** The study successfully demonstrates the potential of utilizing PCB waste to produce SiC micro-particles, which can enhance the thermal conductivity of cooling media. This approach not only provides a method for recycling electronic waste but also contributes to the development of more efficient cooling systems. **Novelty/Originality of this article:** This research introduces an innovative approach to recycling electronic waste by converting PCB waste into valuable SiC micro-particles, offering a novel method for improving cooling media in industrial applications.

**KEYWORDS:** ball to powder ratio; dry milling; particle size; PCB; SiC.

## 1. Introduction

In the current era, where digital advancements permeate various fields, the demand for Electrical And Electronic Equipment (EEE) has drastically increased due to rapid technological progress (Khaliq et al., 2014). In Indonesia, electronic waste is projected to reach 3,200 kilotons by 2040. This equates to each person contributing approximately 10 kilograms of electronic waste annually. Given these statistics, Waste Electrical and Electronic Equipment (WEEE), or electronic waste (e-waste), has become a concern not only for the government but also for the public due to the hazardous materials it contains (Cui & Zhang, 2008). One of the largest contributors to electronic waste is Printed Circuit Boards (PCBs), which are integral components of electronic devices like mobile phones and

### Cite This Article:

Rehanda, R. A., Mochtar, M. A., & Putra, W. N. (2025). Synthesis of silicon carbide (SiC) micro-particles from PCB waste through dry milling as a candidate for microfluidic particles in quenching media. *Humans and Chemical Regimes*, 2(1), 1-15. <https://doi.org/10.61511/hcr.v2i1.1800>

**Copyright:** © 2025 by the authors. This article is distributed under the terms and conditions of the Creative Commons Attribution (CC BY) license (<https://creativecommons.org/licenses/by/4.0/>).



laptops. PCBs serve as conduits for electrical flow, typically using copper as a conductor, and connect components within electronic circuits. By leveraging this, PCB waste, a significant source of e-waste, can be repurposed as a source of particles in fluids, enhancing the thermal conductivity of quenching media and reducing electronic waste in Indonesia.

However, utilizing PCBs as a fluid additive for quenching media remains challenging and underexplored, particularly in transforming PCBs into nano-sized particles suitable for fluid mixtures via dry milling. Therefore, this research focuses on optimizing the dry milling parameters of PCBs for fluid applications. The study examines variables such as Ball Powder Ratio (BPR), time, and speed in a planetary ball mill using the dry milling method. By experimenting with these parameters, the research aims to identify the optimal BPR, time, and speed to achieve the desired particle size, shape, and SiC compound formation with good thermal conductivity properties.

The scope of this research is confined to the synthesis of silicon carbide compounds from PCB materials through dry milling using a planetary ball mill. The milling time variations are set at 10 and 20 hours, with BPR variations of 1:10, 1:30, and 1:50, and a milling speed of 500rpm. Characterization of PCB particles includes Scanning Electron Microscopy (SEM), Energy Dispersive X-Ray Spectroscopy (EDS), X-Ray Fluorescence (XRF), Particle Size Analysis (PSA), and X-Ray Diffraction (XRD). The objectives of this study are to analyze the mechanochemical effects of PCB particles on the enhancement of silicon oxide phases and silicon carbide formation, to assess the impact of the steel ball-to-PCB particle ratio in dry milling on particle size and phase formation, and to evaluate the influence of milling time on particle size and phase development.

In the manufacturing industry, the milling process plays a crucial role due to its flexibility in production. The productivity, quality, and cost of the final product are directly or indirectly dependent on the tool life during machining processes (Sayyad et al., 2021). The production of nanocrystalline substances and materials has become a widely expanding field in materials science over the past decade, owing to the potential to radically modify the properties of solids in their nanocrystalline state (Gusev & Kurlov, 2008). Ball milling is one of the techniques used to break down a material into a powder, achieving very fine particles (in the nanoparticle size range) and mixing with other materials (Trisnayanti, 2020).

Planetary ball milling is capable of grinding materials down to the nanometer scale. Its characteristics can be observed through its mechanical properties, including the fineness of the product and the reliability of the equipment (Wardhana, 2013). The working principle of planetary ball milling involves placing powdered material into a cylinder made of steel balls, with several balls inside, which rotate continuously. Within the cylinder, the balls collide with each other. As a result of these collisions, the powder introduced into the cylinder is impacted by the balls, causing the particles to break apart. This process continues until the desired particle size is achieved.

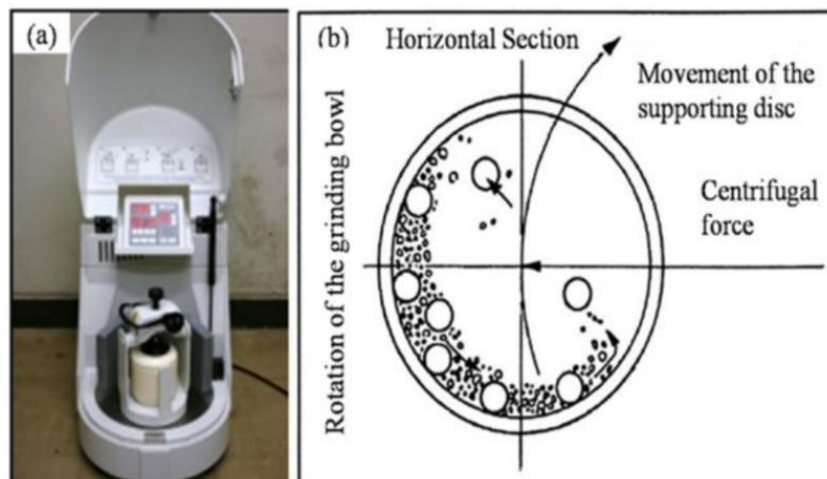


Fig. 1. (a) Planetary ball mill machine (b) Schematic of a planetary ball mill

Dry milling is a traditional comminution technique aimed primarily at reducing particle size (Jing et al., 2015). Smaller particle sizes increase the surface area, thereby enhancing the solubility of materials that are otherwise poorly soluble in water. Dry milling offers advantages such as low operating temperatures and gentle processing conditions, making it a viable option for improving the solubility of particles intended for fluid incorporation. Micro and nanoparticles have been successfully applied across various manufacturing industries. Mechanical milling is a common technique for producing micro and nanoparticles. Therefore, optimizing milling efficiency and quality by determining optimal milling parameters is crucial.

Milling time significantly affects the size and properties of the resulting nanoparticles. Milling is a mechanical process involving the crushing, grinding, or mixing of materials at the nanometer scale using grinding machines or steel balls. Milling speed can significantly influence the size, composition, and properties of the nanoparticles produced. The ball powder ratio (BPR) refers to the ratio of grinding balls to powder in the particle synthesis process. The impact of BPR on nanoparticles can vary depending on the system and process parameters used. Printed Circuit Boards (PCBs) are electronic component boards that form electronic circuits or serve as platforms connecting electronic components without using wires.

Recently, silicon oxide has been considered a promising substitute for elemental silicon due to its abundant reserves, low cost, and ease of synthesis. Additionally, silicon oxide exhibits smaller volume changes during cycling compared to elemental silicon. The atomic structure of SiO has been controversial since its discovery. Philipp proposed a random bonding model, describing SiO as a homogeneous single-phase material with a continuous Si-(OxSi<sub>4-x</sub>) network consisting of randomly distributed Si-Si and Si-O bonds. Brady and Temkin proposed a random mixture model, depicting SiO as a mixture of nanosized amorphous Si and Si<sub>2</sub>O<sub>3</sub>.

Nanoscience is defined as the study of phenomena and manipulation of materials at the molecular and macromolecular scale, which exhibit significantly different properties from larger-scale materials (Hubau et al., 2019). "Nano" refers to a scale of 10<sup>-9</sup>. The definition of nanoparticles depends on the material, field, and application (Hosokawa et al., 2008). Nanoparticles have attracted researchers due to their distinct physical and chemical properties compared to bulk materials, such as magnetic strength, electronic strength, mechanical strength, thermal stability, optical stability, and catalytic stability (Hartmann, 2019).

Microparticles are defined as solid particles with a spherical shape and sizes ranging from 1 to 100 μm. Commercially available microparticles come in various materials, including ceramics, glass, polymers, and metals. Microparticles have a much higher surface-to-volume ratio compared to macro-scale particles, leading to significantly different behaviors. They are predominantly used in the medical field. Microparticles typically appear in three forms in research: discs, rods, and spheres (Bhaskar et al., 2010).

In a study conducted by H. Xie, it was reported that the shape of nanoparticles affects the thermal conductivity of nanofluids (Apmann et al., 2021). The research indicated changes in thermal conductivity due to different shapes of silicon carbide (SiC) nanoparticles suspended in water or ethylene glycol (Munyalo & Zhang, 2018). The size of nanoparticles influences the properties of nanofluids, particularly viscosity and thermal conductivity. In terms of viscosity, relative viscosity decreases as the size of nanoparticles increases (regardless of volume fraction) (Hu et al., 2020).

## 2. Methods

The equipment required for this research begins with the production of PCB nanoparticles, which involves using a blender to reduce the size of the PCBs, followed by disk milling. Before conducting planetary ball milling, the PCBs must first undergo leaching using a beaker glass and a magnetic stirrer. To characterize the fabricated PCB results, SEM equipped with EDS, XRD, and PSA machines are used. Finally, the milling process utilizes a

disc mill, sieves, a mill jar, steel balls, and a planetary ball mill machine. The material used in this research is 1 M HCl for the leaching process of the PCBs. The research flowchart is shown in Fig 2 below.

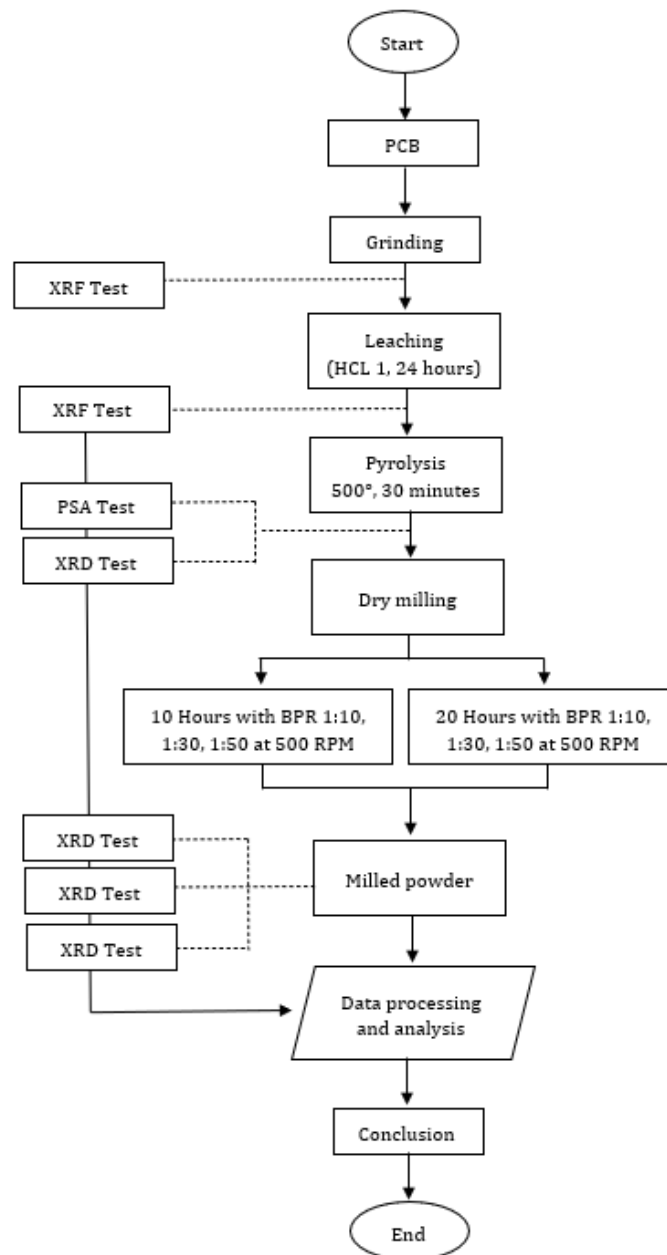


Fig. 2. Research flowchart

This research utilizes milling parameters for nanoparticle formation to understand how these parameters impact the properties of PCB carbon particles and the thermophysical properties of nanofluids. A speed of 500 RPM is used, with time variables set at 10 hours and 20 hours, and BPR variables of 10:1, 30:1, and 50:1.

### 3. Results and Discussion

#### 3.1 Nanoparticle fabrication

The non-metal nanoparticles used in this research are derived from Printed Circuit Boards (PCBs). Initially, the nanoparticles are crushed using a blender. They are then fabricated through a leaching process using 1 M HCl, with a ratio of 600 ml HCl to 100 grams

of PCB powder, for 24 hours. This is followed by pyrolysis using argon gas for 30 minutes at a temperature of 500°C. The final step involves milling with a ball-to-powder ratio of 10:1, 30:1, and 50:1 at a speed of 500 RPM for 10 and 20 hours.

### 3.2 X-ray fluorescence spectroscopy (XRF) analysis

X-Ray Fluorescence Spectroscopy characterization is conducted before and after the leaching process to identify changes in elements and chemical compounds in the PCB material.

Table 1. XRF results before leaching (left) and after leaching (right)

Before Leaching		After Leaching	
Compounds	Percentage (normalization)	Compound	Percentage (normalization)
MgO	19.84%	MgO	6.00%
Al <sub>2</sub> O <sub>3</sub>	9.70%	Al <sub>2</sub> O <sub>3</sub>	10.60%
Cl	0.12%	Cl	5.27%
CaO	21.00%	CaO	20.55%
Fe <sub>2</sub> O <sub>3</sub>	0.65%	Fe <sub>2</sub> O <sub>3</sub>	0.45%
CuO	1.57%	CuO	1.88%
BaO	0.52%	BaO	0.53%
SiO	46.60%	SiO	54.72%
Total	100.00%	Total	100.00%

X-Ray Fluorescence Spectroscopy characterization is conducted before and after the leaching process to identify changes in elements and chemical compounds in the PCB material after the process. Table 1 shows a comparison of X-Ray Fluorescence results before and after leaching. The leaching process is applied to the Printed Circuit Board powder to reduce unwanted metal elements, as the desired nanoparticles are non-metallic. As discussed in Chapter 2 and based on the XRF results in Table 1, the PCB material contains various compounds such as aluminum oxide, magnesium oxide, silicon oxide, chloride, calcium oxide, and copper oxide. According to the tests conducted, before leaching, the sample contained 9.7% aluminum oxide, 19.84% magnesium oxide, 46.6% silicon oxide, 0.12% chloride, 21% calcium oxide, and 1.88% copper oxide.

In Table 1, there is an increase in the element Si and the compound SiO<sub>2</sub>. This trend is likely due to normalization in the XRF results after leaching, which reduces metals that decrease post-leaching, as SiO<sub>2</sub> is a non-metal fraction of the PCB. This is advantageous for the research because the increased SiO<sub>2</sub> suggests a higher likelihood of forming SiC during the subsequent planetary ball milling process. The impact between the powder and steel balls can lead to reactions forming SiC, which has good thermal conductivity for cooling media in fluids (Li et al., 2015). In this study, the reduction of unnecessary metals in the circuit board material aids in producing non-metal nanoparticles. The increase in silicon and silica compounds positively affects the thermal conductivity of nanofluids (Slack, 1964). Silica nanoparticles are mesoporous compounds, which enhance the surface area and distribution, thereby improving the thermal conductivity of nanofluids (Munyalo & Zhang, 2018).

In Table 2, there is a further decrease in the percentage of metal oxide compounds in the PCB powder, along with an increase in some metal oxide compounds, as shown in Table 4.1. For example, Al<sub>2</sub>O<sub>3</sub> decreases from 10.60% to 10.19%, Cl from 5.27% to 2.96%, CaO from 20.55% to 15.32%, and BaO from 0.53% to 0.45%. This occurs because pyrolysis breaks down the polymer chains in PE and PP, forming carbon. Carbon is not detectable by XRF due to its lack of orbitals like metals, leading to percentage normalization in XRF results. However, magnesium oxide shows a significant increase from 6% to 14.65%.

Table 2. XRF results after pyrolysis

Compound	Percentage (normalization)
MgO	14.65%
Al <sub>2</sub> O <sub>3</sub>	10.19%
C1	2.96%
CaO	15.32%
Fe <sub>2</sub> O <sub>3</sub>	0.47%
CuO	1.89%
BaO	0.45%
SiO	54.08%
Total	100.00%

This indirectly affects the balance of oxide composition in the pyrolyzed PCB, with an increase in Mg observed. Another possibility for the rise in MgO after pyrolysis is the decomposition of PP and PE into carbon, altering the density and volume fraction of the constituent oxides.

### 3.3 X-ray diffraction (XRD) analysis

XRD testing is conducted to determine and confirm whether the phases of the compounds in the PCB remain constant or change throughout the various treatment stages. Based on the XRF results of the pyrolyzed PCB powder, several compounds such as metal oxides, chlorides, and the non-metal fraction SiC are still present. Referring to Table 2, the three most abundant compounds in the pyrolyzed PCB powder are SiO<sub>2</sub>, CaO, and MgO. It is assumed that these three compounds should exhibit high peaks or multiple peaks in the XRD graph, as metal oxides still have a significant percentage in the sample and are easily detected by XRD, reflecting more clearly in the XRD results. However, the XRD results after pyrolysis differ from this assumption. As shown in Figure 3, the compound or element with the highest intensity is carbon or charcoal. This phenomenon occurs because one of the components of PCBs is the polymers PP and PE, which have low melting points. Pyrolysis at 500°C breaks down these polymer chains, converting them into carbon or charcoal.

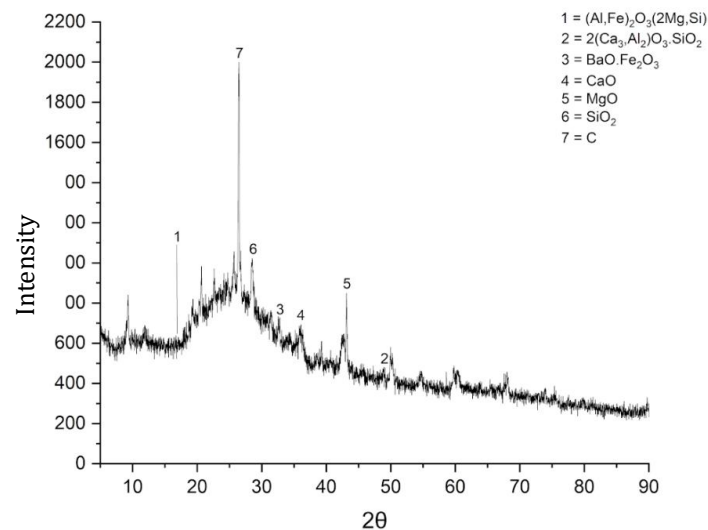


Fig. 3. XRD graphic after pyrolysis

For alkaline earth metal oxides such as BaO, CaO, and MgO, the peak intensity is also quite high because their percentage remains significant after pyrolysis. These oxides are easily detected by XRD. The remaining metal oxides, Al<sub>2</sub>O<sub>3</sub> and Fe<sub>2</sub>O<sub>3</sub>, have lower percentages (Ghosh et al., 2020) and have been somewhat reduced during leaching and pyrolysis, resulting in lower peak intensities, although they are still detectable due to their metallic nature. After pyrolysis, as shown in the XRD graph in Figure 3, it is evident that the

formation of carbon and  $\text{SiO}_2$  is substantial, as these compounds have the two highest peaks and intensities compared to other compounds. Since the goal is to assess whether the subsequent milling process can form the  $\text{SiC}$  compound needed as a mixed particle candidate for quenching media, it is also important to consider the phase equilibrium diagram of  $\text{Si-C-O}_2$ , shown in Figure 4.

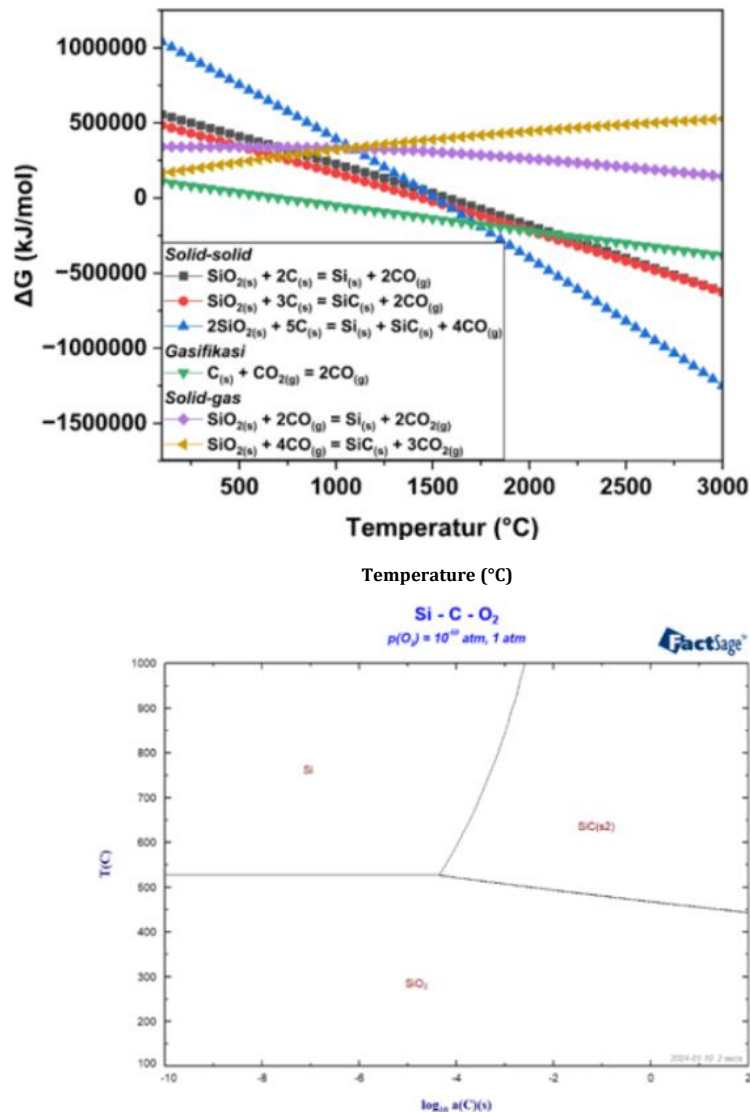


Fig. 4. Si-C-O<sub>2</sub> phase equilibrium diagram and ellingham diagram

In Figure 4, since the most prominent compounds detected by the XRD graph from the PCB powder are  $\text{SiO}_2$  and carbon, a simulation was created using the Fact Sage application to understand how  $\text{SiC}$  forms from  $\text{SiO}_2$  and carbon. The y-axis represents temperature, which in this research context is the kinetic energy generated by the steel balls during milling. As kinetic energy increases, the temperature rises due to the increased collisions between the steel balls, generating heat. This phase equilibrium diagram helps explain and reinforce why  $\text{SiC}$  is the primary phase sought to enhance thermal conductivity in fluids (Lee et al., 2011) as a candidate particle for quenching media, and how it can be formed in this research. After conducting XRD testing at the pyrolysis stage, further testing was performed on the milled samples across six different parameters. The results are shown in Figure 5, which displays the combined XRD graphs from the six milling parameters and the main compounds formed, which are essential for aiding the quenching media.

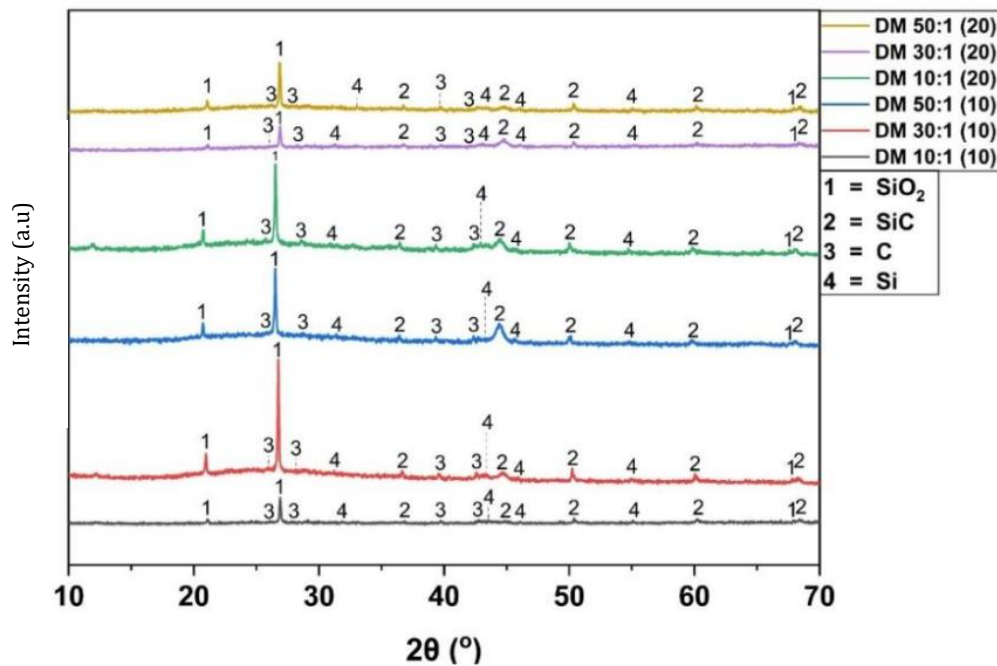


Fig. 5. XRD graphic after milling

Based on the XRD testing results for the 10:1 milling parameter over 10 hours, the overall graph shows low intensity. The main compound,  $\text{SiO}_2$ , has peaks, albeit with low height and intensity, located at 2 theta  $21.131^\circ$  and  $26.953^\circ$ . This indicates that in the smallest ball-to-powder ratio and time parameter,  $\text{SiO}_2$  formation is more significant compared to other compounds like SiC, Si, and C. SiC formation is minimal, with low peaks scattered at several 2 theta angles, the highest intensity being at  $35.73^\circ$ . Referring back to the graph in Figure 4, for the 1:30 ball-to-powder ratio and 10-hour parameter,  $\text{SiO}_2$  formation remains substantial but has decreased, with peaks at 2 theta  $26.686^\circ$  and  $20.904^\circ$ . SiC formation is still minimal, with low peaks at 2 theta  $38.41^\circ$ , while carbon growth is starting to appear with peaks at 2 theta  $26.603^\circ$  and  $42.466^\circ$ . For the 1:50 ratio over 10 hours, a similar trend is observed for  $\text{SiO}_2$  and SiC, but with higher and clearer peak intensities. The SiC peaks are more distinct and higher, aligning with the goal of achieving particles with good thermal conductivity. Table 3 shows the distribution of 2 theta degrees for SiC in each milling parameter.

Table 3. Distribution of 2 theta degrees for sic results

Parameter	2 Theta Degrees of SiC
10 : 1 10 hours	$37,989^\circ$ , $45,494^\circ$ , $60,129^\circ$ , $68,702^\circ$
30 : 1 10 hours	$37,423^\circ$ , $45,276^\circ$ , $60,176^\circ$ , $68,783^\circ$
50 : 1 10 hours	$37,963^\circ$ , $45,095^\circ$ , $59,705^\circ$ , $68,783^\circ$
10 : 1 20 hours	$44,769^\circ$ , $49,321^\circ$ , $61,450^\circ$ , $68,783^\circ$
30 : 1 20 hours	$37,53^\circ$ , $45,31^\circ$ , $51,5^\circ$ , $61,572^\circ$
50 : 1 20 hours	$44,769^\circ$ , $49,321^\circ$ , $61,450^\circ$ , $68,783^\circ$

The phenomenon observed after the milled PCB powder was tested with XRD is that the peak readability for SiC actually decreased. Ideally, increasing the ratio of steel balls to powder and extending the milling time should enhance the formation of SiC. This phenomenon can be explained using the graph in Figure 6, which illustrates the phase growth of each main phase in the PCB powder, such as SiC,  $\text{SiO}_2$ , C, and Si, showing fluctuations in percentage in the semi-quantitative analysis obtained from the Highscore application.

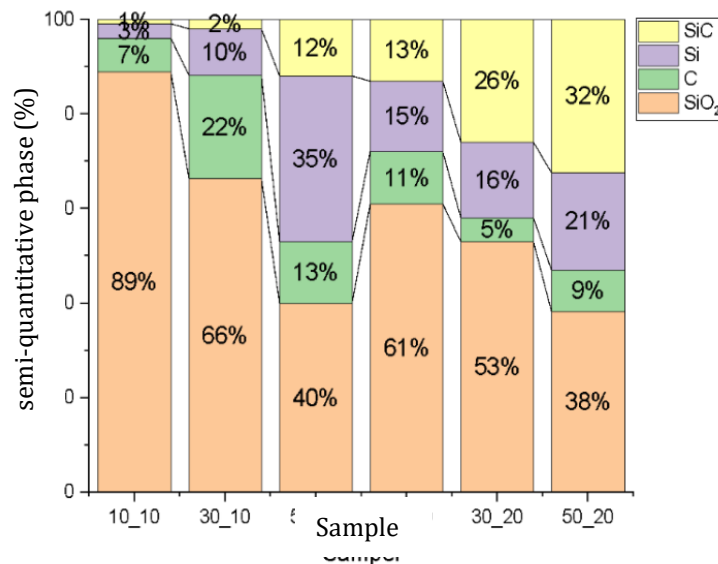


Fig. 6. Phase growth graph results

When observing Figure 6, a pattern or trend in the semi-quantitative percentage of each main phase can be seen. For the graphs with parameters 1:10, 1:30, and 1:50 over 10 hours, the semi-quantitative percentage of SiO<sub>2</sub>, C, Si, and SiC shows an increase in the phases of Si and SiC, and a decrease in the phases of SiO<sub>2</sub> and carbon. This data suggests the hypothesis that adjusting the ratio of steel balls to PCB powder will enhance the formation of Si and SiC phases. According to the chemical reactions, SiO<sub>2</sub> and C, which are the primary raw materials or phases in PCBs, decrease in semi-quantitative percentage as they form the other three phases: solid Si and SiC, and gaseous CO (Hometz et al., 1994).

This phenomenon occurs because SiO<sub>2</sub> is reduced by C to form Si and SiC. With a longer duration of 10 hours compared to previous parameters, SiO<sub>2</sub> continues to form Si and SiC. Additionally, the Si formed from SiO<sub>2</sub> and the existing Si have more time to bond with C to become SiC, aided by the collisions between the steel balls and the powder (Dong et al., 2019). This also affects the temperature and reduces the activation energy required for SiC formation (Zaman et al., 2010), which typically occurs at high temperatures (Wei et al., 2023). Therefore, the mechanochemical process (dry milling) significantly aids in the formation of the SiC phase (Delhaes, 2002; Wang et al., 2012), which has high activation energy, making it more energy-efficient. Increasing the ratio of steel balls to powder can significantly impact Si formation (Wei et al., 2023), and extending the milling time can significantly influence SiC formation (Wei et al., 2023).

The results indicate that SiC shows a positive growth trend in the particles. SiC is an excellent candidate for cooling media due to its superior thermal conductivity (Qin et al., 2019; Wei et al., 2023; Zhang et al., 2014) compared to metallic liquids like sodium and non-metallic liquids like water and oil. The thermal conductivity of SiC is 120–270 W/mK, while other compounds in the particles, such as Si (149 W/mK), C (146–246 W/mK), and SiO<sub>2</sub> (12 W/mK), have lower values. Therefore, SiC is crucial as a candidate particle for cooling media.

### 3.4 Particle size analyzer (psa) analysis

The milled PCB powder is subjected to Particle Size Analyzer (PSA) testing to determine the particle size and distribution for each sample. After testing, the sizes for each sample parameter tested with PSA can be seen in Table 4. The particle size before the milling process was 1077 d.nm, as it had only undergone grinding and disc milling. After milling with a planetary ball mill, there was a significant reduction in particle size across all parameters due to numerous collisions with the steel balls and the high rotation speed of up to 500 RPM, with the disc and vial rotating in opposite directions. Figure 7 shows a trend

where the particle size increases at a ball-to-powder ratio of 1:30 compared to 1:10 and 1:50.

Table 4. PSA testing results

Powder condition	BPR	Time (hours)	Z-Average (d.nm)	Polydispersity index
Before milling	0	0	1077	0.3753
After milling	10:1	10 hours	661.9	0.4277
	30:1	10 hours	710.2	0.1801
	50:1	10 hours	661.2	0.3409
	10:1	20 hours	627.6	0.0470
	30:1	20 hours	864.4	0.3619
	50:1	20 hours	640.4	0.4433

This phenomenon can occur due to two factors. First, the PCB powder undergoing milling will experience extreme collisions with other particles and steel balls. The high speed also increases kinetic energy and automatically raises the temperature in the vial. The PCB powder, known to be primarily composed of  $\text{SiO}_2$ , is quite ductile (Triyono et al., 2020) because, after milling, many particles adhere strongly to the vial sides, indicating ductility. If the powder were rigid, it wouldn't stick to the vial sides. As explained in Chapter 2, during milling, the powder undergoes several phases. First is deformation, where the particle shape changes. Next is the welding phase, where particles fuse, increasing the surface area. The particles then enter the squeezing phase, becoming flattened and changing from ductile to rigid. Once rigid, the final phase is fracturing, where the particles break into smaller sizes.

### 3.5 Scanning electron microscope (SEM) analysis

SEM testing in this study aims to observe and analyze the shape and tendency of particles when not distributed in a fluid. Below are the SEM images from two milling variable results shown in figure.

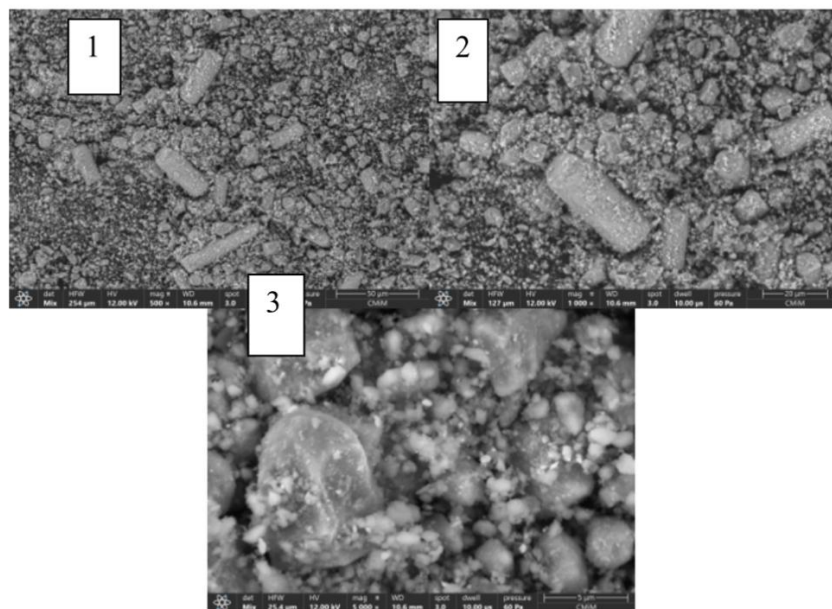


Fig. 7. SEM results 1:50 for 10 hours with magnification (1) 500x (2) 1000x (3) 5000x

In Figure 8, at 1000x and 5000x magnification, many particles have transitioned to a spherical shape rather than cylindrical. This indicates an increased surface area, which positively affects thermal conductivity compared to cylindrical shapes (Wang et al., 2015). Spherical shapes, with their larger surface area, can absorb or conduct more heat, thus exhibiting better thermal conductivity (Tihanyi, 1992; Wu et al., 2015).

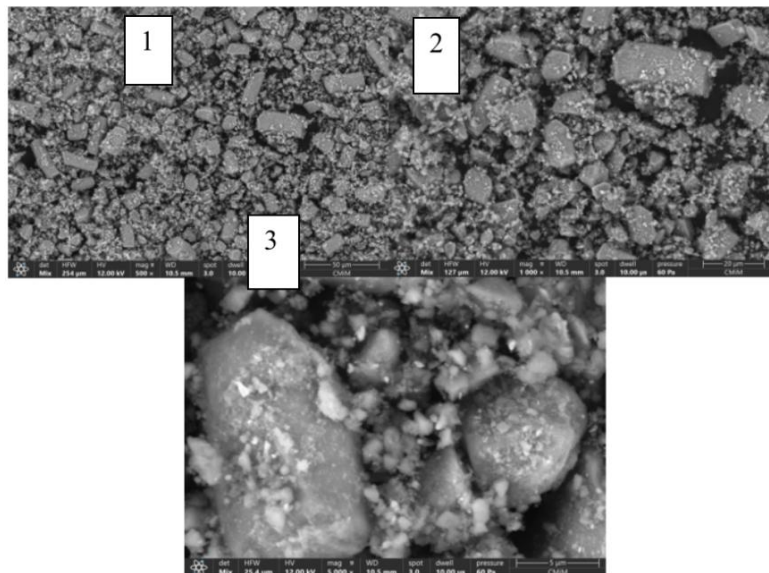


Fig. 8. SEM results 1:50 for 20 hours with magnification (1) 500x (2) 1000x (3) 5000x

Next is the discussion of the EDS results for one of the milled samples. The sample area evaluated with SEM analysis can also be analyzed to identify specific elements using Energy Dispersion Spectroscopy (EDS). X-rays emitted from the sample surface carry unique energy signatures specific to the elements found in the sample. These X-rays are detected by the EDS detector to provide basic information about the sample. EDS provides data on the chemical composition of the sample and additional data about the properties observed in the SEM micrograph. This combined technique is called SEM-EDS or SEM-EDX Analysis. Below are the images and data from the EDS testing.

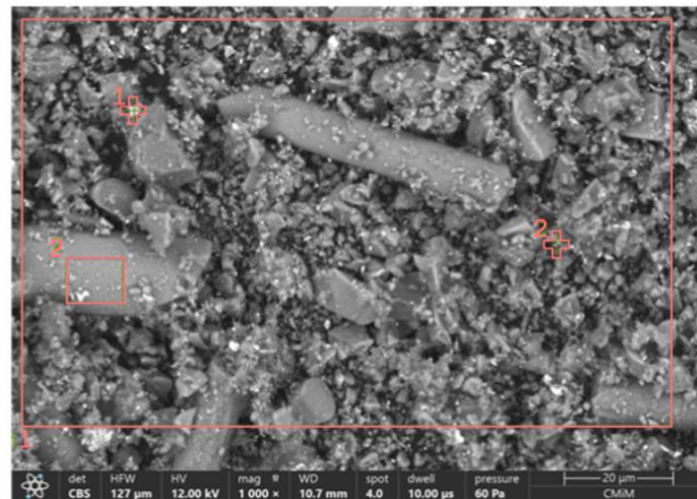


Fig. 9. EDS results

Based on the elemental results detected in the particles, they are predominantly composed of Si, C, O, and Fe. Across the regions and points tested by EDS, the formation of SiC from Si and C is highly likely, as the average percentage of Si across all test areas is 12.475%, and C is 15.05%. Therefore, the potential SiC formation is approximately 12.475%, corresponding to the available Si as a raw material for SiC formation. Other elements still have a presence, consistent with the XRF data, indicating that metals, alkali metals, and alkaline earth metals remain in the particles at low percentages. This data also confirms that SiC formation occurs during the mechanochemical process (dry milling), as evidenced by the EDS analysis.

Table 5. Elemental results from EDS

Element	Atomic %			
	Region 1	Region 2	Point 1	Point 2
S	0.2	0.0	0.0	3.2
C	17.9	11.6	15.7	15.0
O	54.0	55.8	43.6	55.1
Mg	5.7	4.1	6.7	7.5
Al	2.9	3.7	1.9	1.9
Si	13.2	16.4	10.9	9.4
Cl	1.2	0.7	1.0	1.5
Ca	3.6	6.3	1.8	2.4
Fe	0.9	1.3	14.2	0.0
Cu	0.5	0.0	0.0	0.4
Cr	0.0	0.0	4.0	0.0
Ba	0.0	0.0	0.0	3.6

#### 4. Conclusions

Mechanochemistry (dry milling) can influence the formation of silicon and silicon carbide phases, as each parameter consistently shows phase formation through increased semi-quantitative percentages. The ball-to-powder ratio (BPR) affects particle size in the mechanochemical process; a larger BPR does not necessarily result in smaller particles but can transform cylindrical shapes into spheres. BPR significantly impacts the formation of the Si phase, increasing the semi-quantitative percentage from 3% to 35%. The milling time also affects particle size; longer milling does not always yield the smallest particles in this method. The smallest particle size is 627.6 nm with a PDI of 0.047, and milling time influences the crystallinity of the particles. Time significantly impacts the formation of the SiC phase, increasing the semi-quantitative percentage from 1% to 32%. Given that the resulting particle size has not yet reached the optimal range close to 100 nm, several suggestions for future research include focusing on optimizing milling parameters to further reduce particle size and enhance the formation of SiC and C compounds. Additionally, paying closer attention to particle shape could lead to more optimal results.

#### Acknowledgement

The authors express their sincere gratitude to the esteemed reviewers and editors for their valuable time, insightful comments, and constructive suggestions, which have greatly contributed to the improvement of this manuscript.

#### Author Contribution

The authors contributed fully to the writing of this scientific article, from the planning stage to the final editing.

#### Funding

This research received no external funding.

#### Ethical Review Board Statement

Not available.

#### Informed Consent Statement

Not available.

#### Data Availability Statement

Not available.

## Conflicts of Interest

The authors declare no conflict of interest.

## Open Access

©2025. The author(s). This article is licensed under a Creative Commons Attribution 4.0 International License, which permits use, sharing, adaptation, distribution and reproduction in any medium or format, as long as you give appropriate credit to the original author(s) and the source, provide a link to the Creative Commons license, and indicate if changes were made. The images or other third-party material in this article are included in the article's Creative Commons license, unless indicated otherwise in a credit line to the material. If material is not included in the article's Creative Commons license and your intended use is not permitted by statutory regulation or exceeds the permitted use, you will need to obtain permission directly from the copyright holder. To view a copy of this license, visit: <http://creativecommons.org/licenses/by/4.0/>

## References

- Apmann, K., Fulmer, R., Soto, A., & Vafaei, S. (2021). Thermal conductivity and viscosity: Review and optimization of effects of nanoparticles. *Materials*, 14(5), 1–75. <https://doi.org/10.3390/ma14051291>
- Bhaskar, S., Pollock, K. M., Yoshida, M., & Lahann, J. (2010). Towards designer microparticles: simultaneous control of anisotropy, shape and size. *Small*, 6(3), 404–411. <https://doi.org/10.1002/sml.200901306>
- Cui, J., & Zhang, L. (2008). Metallurgical recovery of metals from electronic waste: A review. *Journal of Hazardous Materials*, 158(2–3), 228–256. <https://doi.org/10.1016/j.jhazmat.2008.02.001>
- Delhaes, P. (2002). Chemical vapor deposition and infiltration processes of carbon materials. *Carbon*, 40(5), 641–657. [https://doi.org/10.1016/S0008-6223\(01\)00195-6](https://doi.org/10.1016/S0008-6223(01)00195-6)
- Dong, Y., Li, Y., Zhao, C., Feng, Y., Chen, S., & Dong, Y. (2019). Mechanism of the rapid mechanochemical degradation of hexachlorobenzene with silicon carbide as an additive. *Journal of Hazardous Materials*, 379(January), 120653. <https://doi.org/10.1016/j.jhazmat.2019.05.046>
- Ghosh, P., Marder, R., Berner, A., & Kaplan, W. D. (2020). The influence of temperature on the solubility limit of Ca in alumina. *Journal of the European Ceramic Society*, 40(15), 5767–5772. <https://doi.org/10.1016/j.jeurceramsoc.2020.07.057>
- Gusev, A. I., & Kurlov, A. S. (2008). Production of nanocrystalline powders by high-energy ball milling: Model and experiment. *Nanotechnology*, 19(26). <https://doi.org/10.1088/0957-4484/19/26/265302>
- Hartmann, U. (2019). 18. Nanopartikel. *Materialien, Systeme Und Methoden*, 1, 1–96. <https://doi.org/10.1515/9783110361964-003>
- Hometz, B., Michel, H. J., & Halbritter, J. (1994). ARXPS studies of SiC<sub>2</sub>-SiC interfaces and oxidation of 6H SiC single crystal Si-(001) and C-(001) surfaces. *Journal of Materials Research*, 9(12), 3088–3094. <https://doi.org/10.1557/JMR.1994.3088>
- Hosokawa, M., Nogi, K., Naito, M., & Yokoyama, T. (2008). *Nanoparticle Technology Handbook*. Elsevier. <https://doi.org/10.1016/B978-0-444-53122-3.X5001-6>
- Hu, X., Yin, D., Chen, X., & Xiang, G. (2020). Experimental investigation and mechanism analysis: Effect of nanoparticle size on viscosity of nanofluids. *Journal of Molecular Liquids*, 314, 113604. <https://doi.org/10.1016/j.molliq.2020.113604>
- Hubau, A., Chagnes, A., Minier, M., Touzé, S., Chapron, S., & Guezennec, A. G. (2019). Recycling-oriented methodology to sample and characterize the metal composition of waste Printed Circuit Boards. *Waste Management*, 91, 62–71. <https://doi.org/10.1016/j.wasman.2019.04.041>
- Jing, G., Zhong, Y., Zhang, L., Gou, J., Ji, X., Huang, H., Zhang, Y., Wang, Y., He, H., & Tang, X. (2015). Increased dissolution of disulfiram by dry milling with silica nanoparticles.

- Drug Development and Industrial Pharmacy*, 41(8), 1328–1337. <https://doi.org/10.3109/03639045.2014.949266>
- Khaliq, A., Rhamdhani, M. A., Brooks, G., & Masood, S. (2014). Metal extraction processes for electronic waste and existing industrial routes: A review and Australian perspective. *Resources*, 3(1), 152–179. <https://doi.org/10.3390/resources3010152>
- Lee, S. W., Park, S. D., Kang, S., Bang, I. C., & Kim, J. H. (2011). Investigation of viscosity and thermal conductivity of SiC nanofluids for heat transfer applications. *International Journal of Heat and Mass Transfer*, 54(1–3), 433–438. <https://doi.org/10.1016/j.ijheatmasstransfer.2010.09.026>
- Li, X., Zou, C., Lei, X., & Li, W. (2015). Stability and enhanced thermal conductivity of ethylene glycol-based SiC nanofluids. *International Journal of Heat and Mass Transfer*, 89, 613–619. <https://doi.org/10.1016/j.ijheatmasstransfer.2015.05.096>
- Munyalo, J. M., & Zhang, X. (2018). Particle size effect on thermophysical properties of nanofluid and nanofluid based phase change materials: A review. *Journal of Molecular Liquids*, 265(2017), 77–87. <https://doi.org/10.1016/j.molliq.2018.05.129>
- Qin, X., Li, X., Chen, X., Yang, X., Zhang, F., Xu, X., Hu, X., Peng, Y., & Yu, P. (2019). Raman scattering study on phonon anisotropic properties of SiC. *Journal of Alloys and Compounds*, 776, 1048–1055. <https://doi.org/10.1016/j.jallcom.2018.10.324>
- Sayyad, S., Kumar, S., Bongale, A., Kamat, P., Patil, S., & Kotecha, K. (2021). Data-Driven Remaining Useful Life Estimation for Milling Process: Sensors, Algorithms, Datasets, and Future Directions. *IEEE Access*, 9, 110255–110286. <https://doi.org/10.1109/ACCESS.2021.3101284>
- Slack, G. A. (1964). Thermal conductivity of pure and impure silicon, silicon carbide, and diamond. *Journal of Applied Physics*, 35(12), 3460–3466. <https://doi.org/10.1063/1.1713251>
- Tihanyi, J. (1992). Smart power devices. *Microelectronic Engineering*, 19(1-4), 141–143. [https://doi.org/10.1016/0167-9317\(92\)90409-K](https://doi.org/10.1016/0167-9317(92)90409-K)
- Trisnayanti, N. P. (2020). *Metode sintesis nanopartikel*. Universitas Indonesia.
- Triyono, T., Latief Al Yusron, A., & Surojo, E. (2020). Study Pengaruh Kecepatan Pengadukan pada Proses Stir Casting terhadap Sifat Fisik dan Mekanik AMC Berpenguat Pasir Silica yang Dilakukan Proses Electroless Coating. *Mekanika: Majalah Ilmiah Mekanika*, 19(1), 41–46. <https://doi.org/10.20961/mekanika.v19i1.40248>
- Wang, F., Cheng, L., Xie, Y., Jian, J., & Zhang, L. (2015). Effects of SiC shape and oxidation on the infrared emissivity properties of ZrB<sub>2</sub>-SiC ceramics. *Journal of Alloys and Compounds*, 625, 1–7. <https://doi.org/10.1016/j.jallcom.2014.09.191>
- Wang, H., Sun, S., Wang, D., & Tu, G. (2012). Characterization of the structure of TiB<sub>2</sub>/TiC composites prepared via mechanical alloying and subsequent pressureless sintering. *Powder Technology*, 217, 340–346. <https://doi.org/10.1016/j.powtec.2011.10.046>
- Wardhana, M. V. S. (2013). *Pengaruh kecepatan putar, berat, dan diameter bola pada planetary ball mill sizer terhadap peningkatan produksi zinc oxide*. Universitas Jember. <https://repository.unej.ac.id/handle/123456789/98793>
- Wei, X., Wei, Y., Lu, J., Huang, Y., Sun, Y., Wang, Y., Liu, L., Liu, B., & Han, W. (2023). Evolution of Lewis acidity by mechanochemical and fluorination treatment of silicon carbide as novel catalyst for dehydrofluorination reactions. *Molecular Catalysis*, 537(November 2022), 112948. <https://doi.org/10.1016/j.mcat.2023.112948>
- Wu, R., Zhou, K., Yue, C. Y., Wei, J., & Pan, Y. (2015). Recent progress in synthesis, properties and potential applications of SiC nanomaterials. *Progress in Materials Science*, 72, 1–60. <https://doi.org/10.1016/j.pmatsci.2015.01.003>
- Zaman, S. A. K., Palaniandy, S., & Hussain, Z. (2010). Mechanochemical synthesis of nanostructured SiO<sub>2</sub>-SiC composite through high-energy milling. *Journal of Alloys and Compounds*, 502(1), 250–256. <https://doi.org/10.1016/j.jallcom.2010.04.158>
- Zhang, Z., Du, X., Wang, J., Wang, W., Wang, Y., & Fu, Z. (2014). Synthesis and structural evolution of B<sub>4</sub>C-SiC nanocomposite powders by mechanochemical processing and subsequent heat treatment. *Powder Technology*, 254, 131–136. <https://doi.org/10.1016/j.powtec.2013.12.055>

### Biographies of Authors

**Rifqi Aditya Rehanda**, Department of Metallurgical and Materials Engineering, Faculty of Engineering, Univeritas Indonesia, Depok, West Java, 16424, Indonesia.

- Email: [rifqi.aditya@ui.ac.id](mailto:rifqi.aditya@ui.ac.id)
- ORCID: N/A
- Web of Science ResearcherID: N/A
- Scopus Author ID: N/A
- Homepage: N/A

**Myrna Ariati Mochtar**, Department of Metallurgical and Materials Engineering, Faculty of Engineering, Univeritas Indonesia, Depok, West Java, 16424, Indonesia.

- Email: [myrna.ariati@ui.ac.id](mailto:myrna.ariati@ui.ac.id)
- ORCID: 0000-0002-1711-3867
- Web of Science ResearcherID: N/A
- Scopus Author ID: 58295562200
- Homepage: <https://research.eng.ui.ac.id/researcher/myrnaariati>

**Wahyuaji Narottama Putra**, Department of Metallurgical and Materials Engineering, Faculty of Engineering, Univeritas Indonesia, Depok, West Java, 16424, Indonesia.

- Email: [wahyuaji@ui.ac.id](mailto:wahyuaji@ui.ac.id)
- ORCID: 0000-0002-0294-3606
- Web of Science ResearcherID: KRO-9737-2024
- Scopus Author ID: 57202302947
- Homepage: <https://research.eng.ui.ac.id/researcher/Wahyuaji>